J. Plasma Phys. (2019), *vol.* 85, 905850508 © Cambridge University Press 2019
doi:10.1017/S0022377819000680

Stellarator equilibria with reactor relevant energetic particle losses

Aaron Bader[1],†, M. Drevlak[2], D. T. Anderson[1], B. J. Faber[1], C. C. Hegna[1], K. M. Likin[1], J. C. Schmitt[3] and J. N. Talmadge[1]

[1]University of Wisconsin-Madison, Madison, WI, USA

[2]IPP-Greifswald, Greifswald, Germany

[3]Auburn University, Auburn, AL, USA

(Received 12 July 2019; revised 17 September 2019; accepted 19 September 2019)

Stellarator configurations with reactor relevant energetic particle losses are constructed by simultaneously optimizing for quasisymmetry and an analytically derived metric (Γ_c), which attempts to align contours of the second adiabatic invariant, $J_\parallel$ with magnetic surfaces. Results show that with this optimization scheme it is possible to generate quasihelically symmetric equilibria on the scale of ARIES-CS which completely eliminate all collisionless alpha particle losses within normalized radius $r/a = 0.3$. We show that the best performance is obtained by reducing losses at the trapped–passing boundary. Energetic particle transport can be improved even when neoclassical transport, as calculated using the metric ϵ_{eff}, is degraded. Several quasihelically symmetric equilibria with different aspect ratios are presented, all with excellent energetic particle confinement.

Key words: fusion plasma, plasma simulation, plasma confinement

1. Introduction

In non-axisymmetric equilibria, confinement of guiding-centre orbits is not guaranteed, and enhanced neoclassical losses occur at low collisionality (Galeev *et al.* 1969; Connor & Hastie 1974; Nemov *et al.* 1999). Significant optimization efforts are used to reduce neoclassical losses to acceptable levels (Mynick 2006, and references therein). However, even with good optimization for thermal particle confinement, energetic losses, such as those from alpha particles in stellarator fusion reactors, can be high. Calculations showed that when scaled to a reactor, both the quasihelically symmetric experiment HSX and the quasiaxisymmetric configuration NCSX had a loss of most magnetically trapped alpha particles within a thermalization time (Mynick, Boozer & Ku 2006; Nemov, Kasilov & Kernbichler 2014). In this paper, we look at optimizations specifically targeting energetic particle losses in stellarator equilibria and show that it is possible to generate quasihelically symmetric configurations at the ARIES-CS scale (Najmabadi *et al.* 2008) which reduce energetic particle losses within the mid-radius to below 1 %.

† Email address for correspondence: abader@engr.wisc.edu

Energetic particle confinement has long been thought of as a weak point for stellarators. For example, a simple scaling of the NCSX configuration, a quasiaxisymmetric configuration, to a reactor scale equilibrium (450 m^3 volume at 5.7 T) produced a configuration which lost 27 % of alpha particles promptly, nearly equivalent to the trapped particle fraction (Mynick *et al.* 2006). Prompt losses of this magnitude negatively affect the energy balance and impact ignition requirements. Further optimization of the equilibrium reduced alpha particle energy losses to ∼5 %. However, this level of alpha particle loss was still large enough that the resulting heat flux from alpha particles alone exceeded engineering limits on the divertor plates (Mau *et al.* 2008). These calculations did not include the effects arising from finite coils. Finite coils can give rise to components of the magnetic field spectrum in which the toroidal mode number is a integer multiple of the number of coils. These high-order magnetic field spectral modes can be deleterious to energetic particle confinement. Coil-ripple modes also appear in tokamaks and can produce energetic particle losses. Tokamaks such as ITER include ferritic inserts to reduce energetic particle losses from coil ripple (Tobita *et al.* 2003).

Recent optimizations of a quasiaxisymmetric equilibrium with volume 1900 m^3 and magnetic field on axis of 5 T by Henneberg *et al.* (2019) show losses at normalized toroidal flux $s = \psi/\psi_a = 0.25$ of ≈5 % after 100 ms, when collisions and an electric field are included in the simulation. Here, ψ_a represents the toroidal flux at the edge. The normalized flux s will be used throughout the paper.

In contrast to quasiaxisymmetric equilibria, energetic particle calculations performed by Lotz showed that quasihelically symmetric equilibria could provide improved alpha particle confinement (Lotz *et al.* 1992). Lotz calculated that collisionless alpha particle losses for a quasihelically symmetric (QHS) equilibria with volume 727 m^3 and magnetic field of 5 T were 3 % after 200 ms for $s \approx 0.2$. Lotz also showed that for configurations optimized to eliminate bootstrap current, finite plasma pressure improves confinement. In examining a HELIAS configuration, a reactor scale device based on an early design of W7-X, Lotz found core alpha particle losses were reduced to 10 % at normalized pressure, $\beta = 2\mu_0 P/B^2 = 0.05$ from losses of ≈30 % at $\beta = 0.0$. In the above expression for β, P is the plasma pressure and B is the magnetic field strength.

More detailed calculations of energetic particle losses were also performed for 60 keV protons in W7-X by Drevlak *et al.* (2014). These protons have equivalent normalized gyroradius, $\rho^* = \rho/a$, the ratio of the ion gyroradius to the minor radius, as alpha particles in a device with volume 1800 m^3 and magnetic field on axis of 5 T. It was seen that even in the most optimized configurations of W7-X presented by Drevlak *et al.*, prompt losses at the mid-radius exceeded 10 %. Importantly, these calculations did include the actual magnetic fields produced from coils rather than idealized equilibria.

Losses of energetic particles in non-axisymmetric equilibria come from two sources. The first source is those from the configuration itself as defined by fixed boundary magnetohydrodynamic equilibrium solutions. Generally, any three-dimensional configuration will have particles with non-zero bounce-averaged radial drift. Perfectly axisymmetric configurations are guaranteed to have no direct collisionless orbit losses. However, in all experiments and prototype reactor designs, finite coils are necessary to generate the magnetic field. These coils break axisymmetry in tokamak configurations by providing ‘coil ripple’. Particles can be trapped within local magnetic wells and then subsequently drift radially out of the plasma and escape. In stellarators finite coils will always produce some error by not matching the target boundary exactly.

https://doi.org/10.1017/S0022377819000680 Published online by Cambridge University Press

These errors can produce unwanted terms in the magnetic spectrum, including a coil-ripple term. As in tokamaks, coil ripple in stellarators causes losses due to particles trapped within localized wells. Additionally in stellarators, finite coils can lead to longer wavelength modes in the magnetic spectrum degrading confinement mainly for thermal particles. In this paper, we focus mainly on eliminating the losses from the idealized configuration alone without considering additional losses from finite coils.

The layout of the paper is as follows. In § 2, we discuss the methods we use to optimize stellarator equilibria in general, including a brief introduction to the ROSE code used in this optimization study. Section 3 describes metrics used for optimization of energetic particles in the past, and describes the Γ_c metric that was used to generate the equilibria presented in this paper. Section 4 shows various optimized quasihelically symmetric equilibria that demonstrate excellent confinement of energetic particles, including configurations at different aspect ratios. Finally, § 5 summarizes the results and looks towards the future of energetic particle optimization.

2. Stellarator optimization

Numerous approaches have been developed to reduce neoclassical losses in stellarators (Mynick 2006). One commonly used metric for achieving good neoclassical transport is the effective ripple, ϵ_{eff}, introduced by Nemov in Nemov *et al.* (1999). This metric can be calculated directly from `VMEC` equilibria or from field line following and is the geometric component of the diffusion coefficients in the $1/\nu$ regime, in which the transport increases with decreasing collisionality. In this regime, the perpendicular diffusion, $D_\perp \sim \epsilon_{\text{eff}}^{3/2} v_{dr}^2/\nu$, where v_{dr} is the radial drift velocity and ν is the collision frequency. The collision frequency in this regime is restricted so that it is greater than the poloidal precession frequency due to ∇B and $E \times B$ drifts and less than the bounce frequency of a particle trapped in a local magnetic well. As the radial electric field and the corresponding precession frequency increases, a trapped particle can quickly exit from the $1/\nu$ regime. Nevertheless, the effective ripple is often used as a means of comparing neoclassical transport between various configurations, as seen for example in figure 15 of Spong (2015).

A specific subclass of optimized equilibria, quasisymmetric configurations have tokamak-like neoclassical transport provided there is symmetry in the magnetic field strength. In perfect quasisymmetry there are no particles with net radial drifts and hence no $1/\nu$ neoclassical transport. Designs of quasisymmetric equilibria were generated by Nührenberg & Zille (1988). In practice exact quasisymmetry cannot be attained globally in a stellarator (Garren & Boozer 1991). However, stellarator designs that approximate quasisymmetry generally have favourable neoclassical transport. To date, only one quasisymmetric stellarator has been built and operated, the quasihelically symmetric experiment (HSX) in the University of Wisconsin-Madison (Anderson *et al.* 1995). However, many other quasisymmetric configurations have been examined including NCSX (Zarnstorff *et al.* 2001), ARIES-CS (Najmabadi *et al.* 2008), CHS-QA (Okamura *et al.* 2001) and a more recent adaptation (Liu *et al.* 2018) and also by Henneberg *et al.* (2019).

Besides HSX, the only other operating neoclassically optimized stellarator is the quasi-omnigenous W7-X stellarator in Germany (Klinger *et al.* 2016). W7-X was designed as a quasi-omnigenous device and did not target quasisymmetry. Instead, the design targeted a number of physics properties including reduced Pfirsch–Schlüter and bootstrap currents consistent with reduced neoclassical transport.

https://doi.org/10.1017/S0022377819000680 Published online by Cambridge University Press

2.1. *Boundary optimization*

Finding equilibria that possess good neoclassical transport, whether through quasisymmetry or other optimizations is not trivial. While various schemes are being pursued such as an analytic construction from first principles (Landreman & Sengupta 2018), the conventional method, and the one used to design HSX, W7-X, and NCSX, is to couple a nonlinear boundary optimization with an equilibrium solver. In this optimization scheme, the plasma boundary is parametrized in Fourier modes, such that,

$$R = \sum_{m,n} R^c_{m,n} \cos(m\theta - n\zeta) + R^s_{m,n} \sin(m\theta - n\zeta) \tag{2.1}$$

$$Z = \sum_{m,n} Z^c_{m,n} \cos(m\theta - n\zeta) + Z^s_{m,n} \sin(m\theta - n\zeta). \tag{2.2}$$

Here m is a poloidal mode number, n is a toroidal mode number, θ is the poloidal angle and ζ is the toroidal angle. An additional restriction can be imposed, called 'stellarator symmetry' where $Q(R, \phi, Z) = Q(R, -\phi, -Z)$ for any function Q. Imposing stellarator symmetry eliminates all the R^s and Z^c components, and only the cosine terms are left in the equation for R and the sine terms in the equation for Z. That is

$$R(\theta, \zeta) = \sum_{m,n} R_{m,n} \cos(m\theta - n\zeta), \tag{2.3}$$

$$Z(\theta, \zeta) = \sum_{m,n} Z_{m,n} \sin(m\theta - n\zeta), \tag{2.4}$$

where the superscripts have been dropped. All the quasihelically symmetric configurations in this paper will have four stellarator symmetric field periods, $n = 4n_k$, $n_k = 0, 1, 2, \ldots$.

For a given boundary, along with specification of the flux surface profiles for plasma pressure and toroidal current, the equilibrium can be calculated assuming ideal magnetohydrodynamics. Current optimization tools use the variational moments equilibrium code (`VMEC`) to solve for the equilibrium (Hirshman & Whitson 1983).

With knowledge of the shapes of all equilibrium flux surfaces, it is possible to calculate performance, F, by quantifying the configuration's ability to attain prescribed metrics. For example, it is often convenient to calculate the performance with respect to many metrics in the least-squares format as is used in `ROSE` (described in more detail below),

$$F(\{R_{mn}, Z_{mn}\}) = \sum_i w_i [p_i(\{R_{mn}, Z_{mn}\}) - t_i]^2. \tag{2.5}$$

In (2.5) each p_i represents a penalty function that evaluates the performance with respect to a given metric. The desired targets are given by t_i and each function is weighted by w_i. The performance of the equilibrium with respect to all weighted penalty functions is used to calculate better equilibria in a global optimization scheme. In the rest of this section we will first look at some equilibrium properties that will be used in various optimization calculations, and then we will briefly discuss the global optimization scheme.

https://doi.org/10.1017/S0022377819000680 Published online by Cambridge University Press

2.2. *Metrics for equilibrium performance*

In principle any quantity that is calculable from a plasma equilibrium can be used as a penalty function. Here, we outline some basic equilibria quantities that we will use in the global optimizations presented in this paper.

We specify basic features of the plasma in order to ensure that the equilibrium does not diverge far from the starting configuration. In the following, we optimize by fixing the aspect ratio and major radius. For the purpose of comparing energetic particle confinement between configurations, we scale the equilibrium to ARIES-CS volume and magnetic field strength.

An important metric for the optimizations presented here is the degree of quasisymmetry. For a given flux surface, this is defined as the amount of magnetic energy in non-symmetric modes compared to symmetric modes. The calculation is achieved by first transforming coordinates from `VMEC` coordinates to Boozer coordinates (Boozer 1982). After this is done, the magnetic field on the surface is given as

$$B(\theta^B, \zeta^B) = \sum_{m,n} B_{m,n} \cos(m\theta^B - n\zeta^B), \tag{2.6}$$

where θ^B and ζ^B are the poloidal-like and toroidal-like coordinates in Boozer coordinates. Only the stellarator symmetric components are considered.

For a four period quasihelically symmetric configuration, the quasisymmetric modes are those where $n/m = 4$. Therefore the quasisymmetric penalty to minimize is

$$P_{\text{qhs}} = \left(\sum_{n/m \neq 4} B_{m,n}^2 \right) \Big/ B_{00}^2. \tag{2.7}$$

The division by the $m = 0$, $n = 0$ mode is used for normalization purposes.

The rotational transform, or ι, profile is a very commonly specified parameter. In the optimizations presented in this paper it is always left as a free parameter. It is important to remember that `VMEC` cannot include the effects from magnetic islands, so equilibria will not be penalized for producing profiles that pass through resonant surfaces. In particular it is important to avoid the low-order rational surfaces, such as the $\iota = 1$ surface. At these surfaces, not only is it expected to have large islands, but construction of Boozer coordinates is ill posed and quasisymmetry, along with other metrics, cannot be properly assessed. Avoiding such surfaces is not guaranteed if the rotational transform profile is unconstrained. For all the configurations shown here, the configurations have rotational transform, $1 < \iota < 4/3$.

With the exception of energetic particle metric Γ_c described below, the equilibrium optimization is attempted with the above equilibrium penalties. We attempt to minimize the quasisymmetric penalty, and we do not constrain the rotational transform profile. We also constrain neoclassical transport by ensuring that the ϵ_{eff} metric described above does not exceed a target value. In practice, good quasisymmetric properties ensure good neoclassical transport, and thus the ϵ_{eff} constraint is never exceeded in these optimizations.

2.3. *Optimization*

Optimization for the configurations in this paper are carried out with `ROSE` (ROSE optimizes stellarator equilibria) (Drevlak *et al.* 2018).

https://doi.org/10.1017/S0022377819000680 Published online by Cambridge University Press

The global optimizer seeks to minimize the function given in (2.5). The optimizer varies the boundary coefficients, $\boldsymbol{R}_c$ and $\boldsymbol{Z}_s$ in the VMEC parametrization, in an attempt to find a new configuration with a lower value of F. Specifically, for these optimizations we use Brent's algorithm (Brent 2013).

The optimization method, like many optimization methods, is subject to local minima problems preventing further improvements of the metrics. A local minimum exists where all small perturbations of the boundary coefficients, $\boldsymbol{R}_c$ and $\boldsymbol{Z}_s$ result in a larger value of F. Areas of phase space can exist far away with lower values of F, but the optimizer cannot reach them along any local gradient descent path. For more information on optimization with ROSE the reader is directed to Drevlak *et al.* (2018).

3. The Γ_c for energetic particle confinement

Optimization for energetic particles is a necessity for stellarator reactor configurations. The simplest optimization metric, for isotropically distributed particles such as alpha particles, is to use Monte Carlo methods. The Monte Carlo analysis is done by launching a population of energetic particles, following the particle orbits, and determining the fraction of particles that are lost. There are numerous options for the analysis including whether to use guiding-centre approximations or full-orbit calculation, whether to include collisions, and various choices involving the starting distribution of particles. Integrating the guiding-centre drift orbit equations is fast enough that it is feasible to implement Monte Carlo methods into an optimization scheme for some moderate number of particles and short time scales of the order of several hundred toroidal transits. This was the approach taken by Ku and Garabedian to optimize the NCSX equilibrium (Ku & Garabedian 2006) (also see description in Mynick *et al.* 2006).

Instead of optimizing with Monte Carlo techniques, we employ an analytical metric for energetic particle confinement and then use particle following to evaluate the resulting optimized configuration. Optimizing with fast-particle metrics rather than with Monte Carlo has two advantages. The first is that the computational cost is significantly lower, allowing for many separate optimizations with different targets and weights. The second advantage is that the metrics include physics insights directly, rather than requiring analysis of the resulting configurations to determine why one configuration performs better than another.

A question to address is whether improved energetic particle confinement is correlated to improvements in neoclassical transport (ϵ_{eff}) and/or quasisymmetry. The ϵ_{eff} metric by virtue of providing better neoclassical transport of thermal particles, might also provide improved confinement of energetic particles. Similarly, a perfectly quasisymmetric configuration will confine all particles, so the quasisymmetry metric can also be used as an energetic particle method. As will be shown in § 4, improvements to energetic particle confinement do not always imply lowered values of ϵ_{eff}. On the other hand, improving quasisymmetry does improve energetic particle behaviour. Nevertheless, we find that the best performance is obtained by considering the Γ_c metric, which will be described presently.

Instead of optimizing for quasisymmetry or ϵ_{eff}, Nemov proposed creating poloidally closed contours of the second adiabatic invariant, $J_\parallel = \oint v_\parallel \mathrm{d}s$ by examining both the radial and poloidal drifts (Nemov *et al.* 2005, 2008). Differentiation of J at constant energy provides the bounce-averaged radial and poloidal drifts (Helander *et al.* 2012). That is,

$$\left\langle \frac{\mathrm{d}\psi}{\mathrm{d}t} \right\rangle = \frac{1}{Ze\tau_b}\frac{\partial J}{\partial \alpha}; \quad \left\langle \frac{\mathrm{d}\alpha}{\mathrm{d}t} \right\rangle = \frac{1}{Ze\tau_b}\frac{\partial J}{\partial \psi}, \tag{3.1a,b}$$

https://doi.org/10.1017/S0022377819000680 Published online by Cambridge University Press

where the magnetic field, $\boldsymbol{B} = \nabla\psi \times \nabla\alpha$, Ze is the particle charge and τ_b is the bounce time. Therefore, if $J = J(\psi)$ the radial drift is eliminated and the particle is confined. The specific innovation by Nemov is an analytic method of calculating both the radial drift of the particles, which is a quantity to minimize, and the poloidal drift of the particles, a quantity to maximize. By maximizing the poloidal drift in non-axisymmetric equilibria, it is possible to align the $J_\parallel$ contours with the flux surfaces (Mikhailov *et al.* 2002) in a more direct manner than possible by previously explored proxies such as J^* (Cary, Hedrick & Tolliver 1988; Spong *et al.* 1998). In the limit of $\iota/N \ll 1$, $J^* \approx J$. Here, N is the number of field periods. This proxy is well suited for higher field period, moderate transform devices, but less well suited for quasihelically symmetric devices, such as the ones considered in this paper where $\iota/N \approx 1/4$.

The metric we optimize is given in (61) in Nemov *et al.* (2008). The Γ_c metric is given as

$$\Gamma_c = \frac{\pi}{\sqrt{8}} \lim_{L_s\to\infty} \left(\int_0^{L_s} \frac{\mathrm{d}s}{B} \right)^{-1} \left[\int_1^{B_{\max}/B_{\min}} \mathrm{d}b' \sum_{\text{well}_j} \gamma_{cj}^2 \frac{v\tau_{b,j}}{4B_{\min}b'^2} \right], \tag{3.2}$$

where γ_c is

$$\gamma_c = \frac{2}{\pi} \arctan\left(\frac{v_r}{v_\theta}\right). \tag{3.3}$$

Here, v_r is the bounce-averaged radial drift, v_θ is the bounce averaged poloidal drift. The ratio v_r/v_θ is calculated from geometrical quantities of the magnetic field line and is described in (51) in Nemov *et al.* (2008) (we ignore the electric field contribution and set the arbitrary reference field $B_0 = B_{\min}$). The sum is taken over all the wells on a suitably long field line. For this calculation 60 toroidal transits were used. The calculation considers trapping wells encountered by all possible trapped particle pitch angles, with b' representing a normalized value of the reflecting field. The bounce time for a particle in a specific magnetic well is given by $\tau_{b,j}$. The parameters $B_{\max}$ and $B_{\min}$ are the maximum and minimum magnetic field strength on the flux surface. Succinctly, the key quantity to minimize is the ratio of the drifts, v_r/v_θ.

It is important to highlight the difference between ϵ_{eff} and Γ_c; both of which were introduced by Nemov. The effective ripple, ϵ_{eff}, targets deeply trapped particles that dominate transport in the $1/\nu$ regime and is weighted by the collision operator. However, energetic particle confinement is influenced over a wider range of pitch angles, especially at angles near the trapped/passing boundary. Γ_c, as mentioned above, represents the angle between the J contours and magnetic flux surfaces. Unlike ϵ_{eff}, Γ_c is collisionless. An objective of this study is to use the Γ_c metric to see how far one can improve the confinement of energetic particles, while still providing a ceiling for ϵ_{eff}, but not deliberately optimizing ϵ_{eff} to get as small a value as possible. Details of the optimization process will be described at the beginning of § 4.

3.1. *Evaluation of energetic particle losses*

To evaluate a given configuration we use a Monte Carlo scheme using the `ANTS` code (Drevlak *et al.* 2014). `ANTS` integrates the drift orbit of particles on a user defined magnetic grid and can include collisions. In these calculations collisions are turned off, and the magnetic grid extends only to the `VMEC` boundary after which particles are presumed lost. In order to ensure the launched particles match an experimentally

https://doi.org/10.1017/S0022377819000680 Published online by Cambridge University Press

relevant distribution of particles some precautions are necessary in the launch profiles. It is assumed that density and temperature are flux functions. For a given surface s_0, particles are launched from random surface coordinates (θ, ζ) so that the probability of finding a particle in any given volume element, $\mathrm{d}V_0$ centred at (s_0, θ_0, ζ_0) is proportional to $\mathcal{J}(s_0, \theta_0, \zeta_0)$, where $\mathcal{J}$ is the three-dimensional Jacobian. This leads to a launch population that, for a given flux surface, is equivalent to the alpha particle production in a burning plasma.

Similarly it is necessary to ensure an isotropic distribution in velocity space. This is easily done by choosing the parallel velocity, $v_\parallel = v\sin(\alpha)$, for each particle randomly from a uniform distribution between $-v$ and v. Here α is the pitch angle of the particle velocity vector with magnitude v.

For all calculations in this paper we consider 5000 particles per flux surface. For each particle, the particle location and velocity vectors are determined randomly as described above. Because of the isotropic distribution, a significant number of particles are passing particles.

In ANTS, a magnetic grid in cylindrical coordinates is computed. Particle following is accomplished by integrating guiding-centre orbit equations in these cylindrical coordinates. The integration method is a fourth-order Adams–Bashforth scheme. For this calculation we do not consider particle collisions. If the particle trajectory passes beyond the boundary of the penultimate flux surface, it is considered lost. For the results in this paper, particles are followed for 200 ms, and any particle that does not pass beyond the penultimate flux surface in 200 ms is considered confined. For reference, the bounce time for an alpha particle near the trapped passing boundary for these configurations is approximately 0.1 ms.

Basic analysis was performed to ensure Monte Carlo scaling and error estimates by repeating 10 simulations with different randomized launch profiles. It was verified that the standard deviation scales with $\sqrt{N}$ where N is the number of particles. For a configuration with approximately 10 % alpha particle losses, the standard deviation is 0.32 %. This produces a roughly 3 % error in the lost particle subpopulation due to Monte Carlo noise.

4. Results and discussion

The starting configuration for analysis is a quasihelically symmetric configuration with aspect ratio 6.7. After optimization, we scale the configurations to ARIES-CS parameters with plasma volume of 450 m^3 and magnetic field of 5.7 T on axis. For these optimizations, we specify the major radius and aspect ratio and do not allow either to vary. We also constrain ϵ_{eff} to lie below some nominal value (here 0.01). We optimize for three cases, the first is an optimization only attempting to improve the quasisymmetry at normalized toroidal flux, $s = 0.6$. The second attempt optimizes for Γ_c at three surfaces, $s = 0.2$, 0.4 and 0.6. The third attempt optimizes both the quasisymmetry metric (at $s = 0.6$) and the Γ_c metric (at $s = 0.2$, 0.4 and 0.6) simultaneously.

Figure 1(*a*) shows the values for the quasisymmetric metric computed for each of the four optimization cases and plotted as a function of s. For these results and all similar plots, even though the values may have been optimized on only one surface (for QHS) or three surfaces (for Γ_c) we show the values of the metric at surfaces between $s = 0.1$ and $s = 0.7$. The two optimizations that include quasisymmetry as a penalty, (orange and red) show lower values of quasisymmetry over the entirety of the minor radius, except possibly in the very core. Note the broad reduction despite that

https://doi.org/10.1017/S0022377819000680 Published online by Cambridge University Press

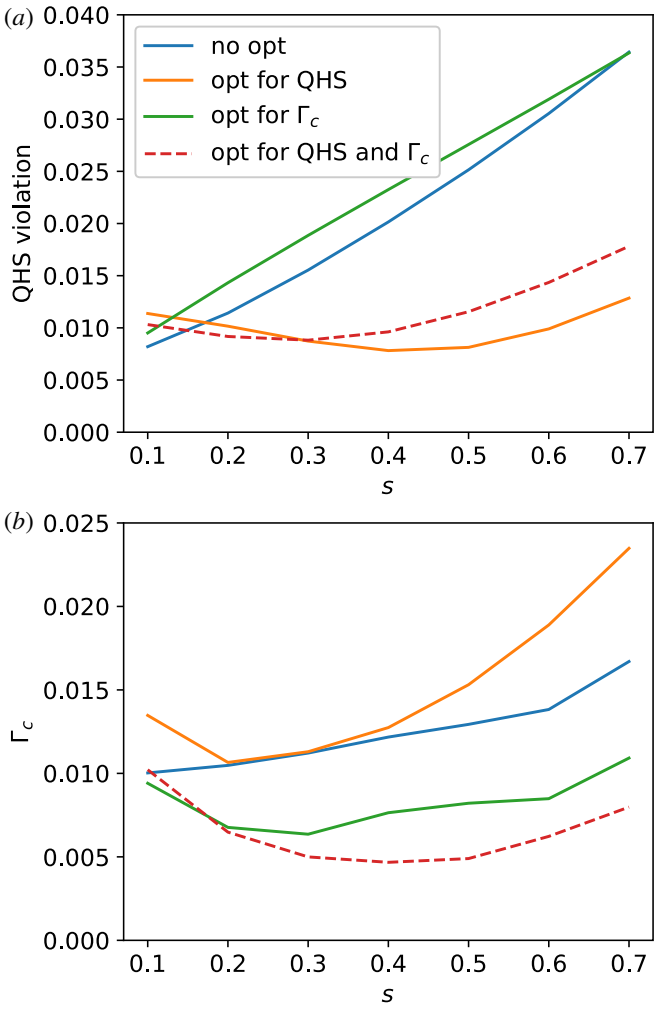

FIGURE 1. The quasisymmetric metric (*a*) from (2.7) and Γ_c (*b*) metric from (3.2) as a function of normalized toroidal flux for four different optimization targets.

the optimization only targeted quasisymmetry at $s = 0.6$. This behaviour is typical for optimization for quasisymmetry.

Figure 1(*b*) shows a similar plot, but this time the Γ_c metric is plotted as a function of s. Again the two cases that included the Γ_c metric in the optimization (green and red) show lower values of Γ_c across most of the plasma. It appears from this result that the quasisymmetric metric and Γ_c can be optimized separately. Indeed, the following four configurations provide a good test case for comparing the behaviour of these two metrics on energetic particle confinement. The flux surfaces for the four configurations are shown in figure 2(*a*). The rotational transforms for the four configurations are shown in figure 2(*b*). The results show that even though the rotational transform was not explicitly targeted in the optimization, the configurations have rotational transforms between the low-order rational surfaces of $\iota = 1$ and $\iota = 1.25$.

https://doi.org/10.1017/S0022377819000680 Published online by Cambridge University Press

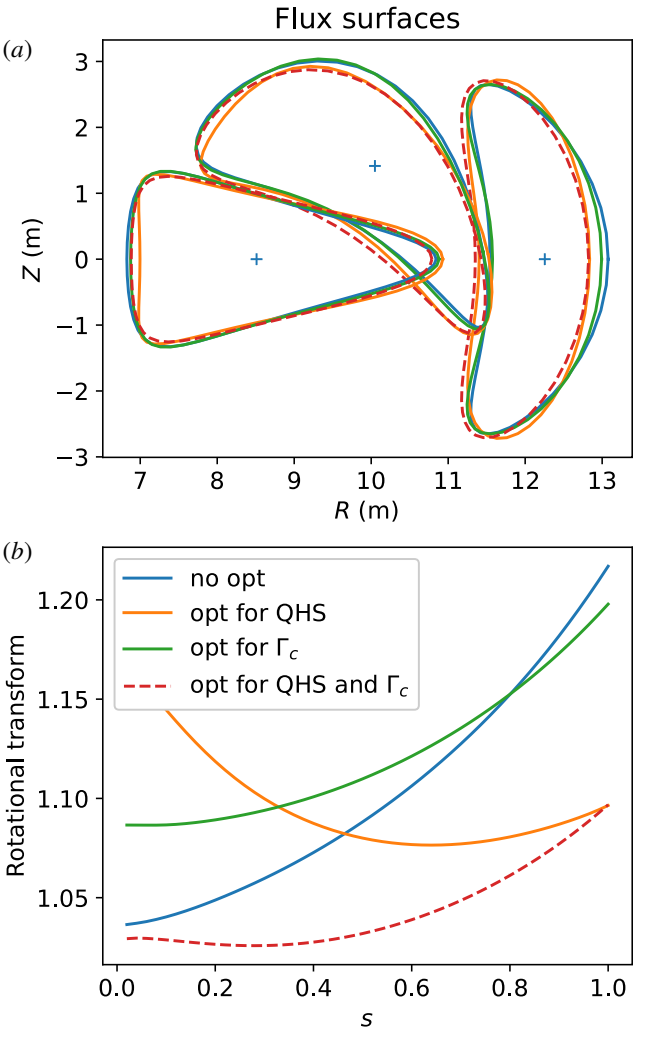

FIGURE 2. Flux surfaces are shown at toroidal cuts at $\phi = 0$, $\pi/8$ and $\pi/4$ (*a*). The magnetic axis is shown for the unoptimized case as a blue '+'. The colours in this plot use the same legend as in the bottom plot. Panel (*b*) shows the rotational transform as a function of normalized toroidal flux for four different optimization targets.

The evaluation for energetic particles is shown for particles beginning on the $s = 0.1$, 0.3 and 0.4 flux surfaces in figure 3. In the core, at $s = 0.1$ (figure 3*a*) corresponding to normalized minor radius, $r/a \sim 0.32$, all configurations show losses below 4 % after 200 ms. The best performing case (red dashed) completely eliminates all alpha particle losses on this flux surface. For all configurations after about 10 ms the particle loss fraction is saturated.

Further out, at $s = 0.3$ (figure 3*b*), corresponding to $r/a \sim 0.54$, some differences can be seen between the four cases. The best performing case (red dashed) again shows low losses. No particles are lost before about 20 ms, and less than 1 % loss exists after 200 ms. The other configurations perform worse both with regard to prompt losses and after long time scales. All three other cases show approximately

https://doi.org/10.1017/S0022377819000680 Published online by Cambridge University Press

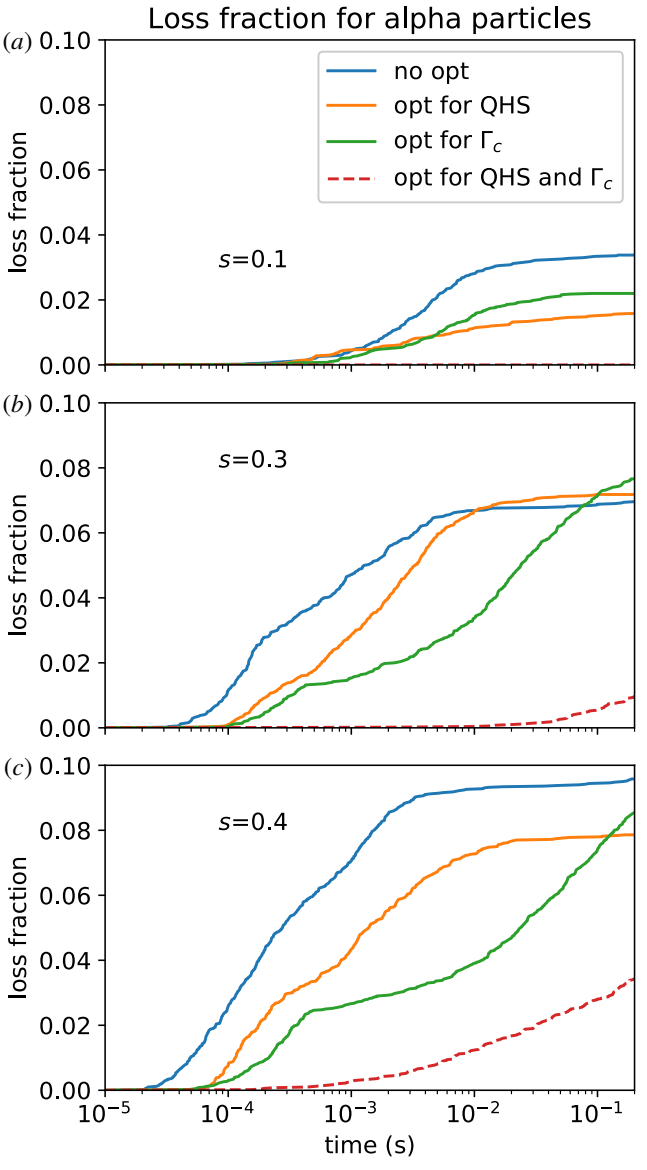

FIGURE 3. Alpha particle loss fractions for alpha particles born on the $s = 0.1$ (a), $s = 0.3$ (b) and $s = 0.4$ (c) surfaces as a function of time for four different optimization cases.

7 % loss after 200 ms. Interestingly a clear difference appears in the time behaviour between the configuration optimized for Γ_c (green) and the unoptimized case (blue) and the case optimized for quasisymmetry (orange). After 10 ms, the optimization for Γ_c (green) performs significantly better than the other two, indicating an improvement in confining prompt losses of particles. However after 200 ms it performs slightly worse.

The trends continue further out at $s = 0.4$ (figure 3c), corresponding to $r/a \sim 0.63$. At $s = 0.4$, the losses from the configuration with optimization for Γ_c and quasisymmetry is about 1 % after 10 ms and 3 % after 200 ms. Similar behaviour is

https://doi.org/10.1017/S0022377819000680 Published online by Cambridge University Press

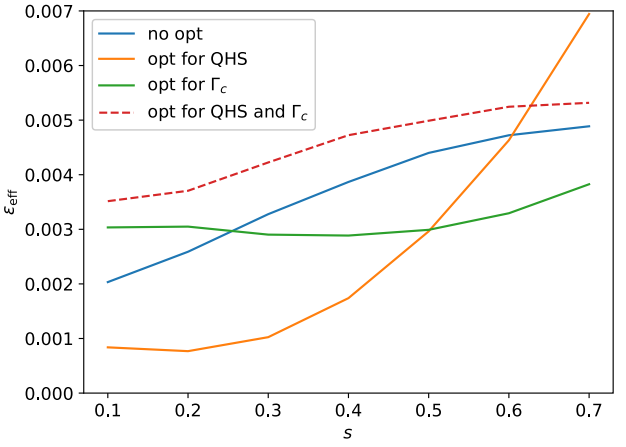

FIGURE 4. The ϵ_{eff} metric as a function of normalized toroidal flux for four different optimization targets.

seen with the case optimized for Γ_c where it reduces prompt losses, but after 200 ms performs equivalently to the other two cases with approximately 8 % losses.

It is clear from these results that quasihelically symmetric configurations exist that have VMEC equilibria that eliminate all alpha particle losses within $s = 0.1$ on an ARIES-CS scale device. The configuration was obtained with a basic set of optimization targets, using only the quasisymmetry metric and the Γ_c metric.

We now turn towards some of the features of the optimized equilibria. One of the basic results is that improvements to energetic particle confinement are not correlated to improvements in neoclassical transport given by ϵ_{eff}. In figure 4 we show the computed values of ϵ_{eff} for the four optimization configurations, which demonstrates that the optimization which produced the best energetic particle confinement actually has the worst predicted neoclassical transport over the inner half of the plasma. It should be noted, that more accurate neoclassical calculations are available, such as with SFINCS (Landreman *et al.* 2014). These calculations have not been undertaken for these configurations. Rather the conclusion here is with regard to the limitation of ϵ_{eff} as a useful metric for energetic particles.

It is also useful to look at the loss as a function of the value of field that the alpha particle will reflect at, E/μ, which is directly related to the particle's pitch angle. The results for $s = 0.3$ and $s = 0.4$ are shown in figure 5. For both cases only trapped particles are lost, which is expected. Two more interesting features are apparent from the results presented here. The first is that for all configurations the losses are predominately from particles near the trapped–passing boundary. These losses are significantly reduced when Γ_c and quasisymmetry are both optimized for (red). However, in this best performing case there are some losses of deeply trapped particles at $s = 0.4$. This may be expected due to the degradation of ϵ_{eff} in this case. In other words, the optimizer sacrificed some confinement of deeply trapped particles to improve confinement of energetic particles near the trapped–passing boundary. This is a good trade-off for particles born uniformly on flux surfaces, like alphas. Deeply trapped particles can only be born in areas of low magnetic field, while barely trapped particles can be born at all locations on the flux surface.

Comparing this optimization attempt with previous attempts by Ku & Garabedian (2006) and Nemov *et al.* (2014) yield some insights. In this optimization, the original

https://doi.org/10.1017/S0022377819000680 Published online by Cambridge University Press

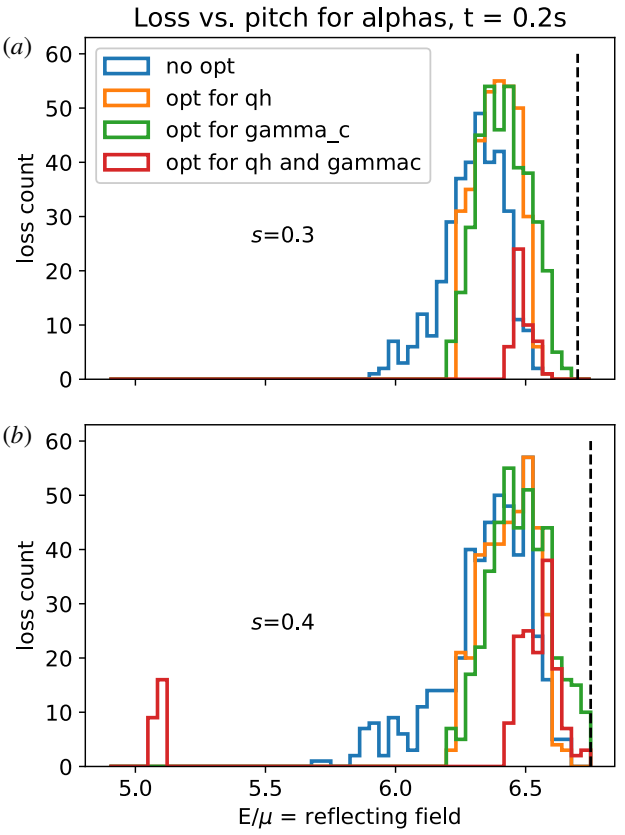

FIGURE 5. Loss counts as a function of reflecting field (E/μ) for alpha particles for four different optimizations. Values are calculated for particles launched at flux surfaces $s = 0.3$ (a) and $s = 0.4$ (b). The black vertical dashed line in each plot represents the trapped–passing boundary.

equilibrium is a scaled version of NCSX and suffered from energetic particle losses at all pitch values. A salient feature of the optimized equilibrium was the removal of magnetic wells at intermediate pitch values, thus producing a class of confined energetic particles. However, this process degraded quasisymmetry and introduced mirror modes, that is modes in the magnetic spectrum with poloidal number, $m = 0$ and toroidal number $n \neq 0$. For the quasihelically symmetric configurations in this paper, there are very few losses at intermediate field values (see figure 5, $5.2 < E/\mu < 6.0$). Therefore, there are no improvements to be had by improving confinement in these regions of phase space since the particles are already well confined.

A different optimization by Nemov *et al.* (2014) attempted to remove losses due to coil-ripple effects. They showed that in HSX, the transition from an idealized quasisymmetric equilibrium to one produced from realistic coils significantly reduced energetic particle confinement. However, by doubling the number of coils from 48 to 96 using a simple interpolation scheme, the original good confinement was recovered. This occurred even though the new coils were not optimized and quasisymmetry was degraded in the 96 coil configuration.

https://doi.org/10.1017/S0022377819000680 Published online by Cambridge University Press

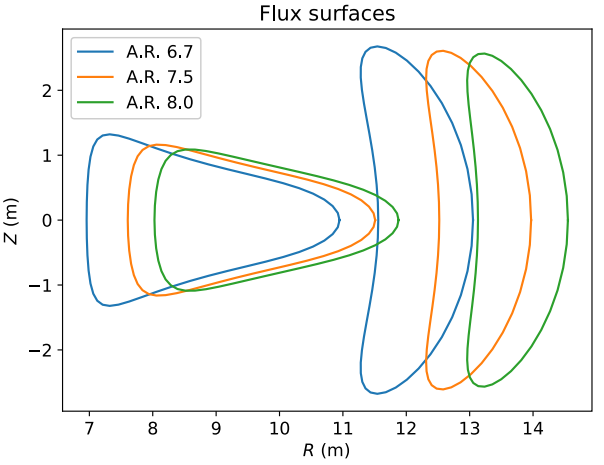

FIGURE 6. Boundary flux surfaces for the bean ($\phi = 0$) and triangle ($\phi = \pi/4$) surfaces for three optimized configurations with different aspect ratios.

4.1. *Optimization at higher aspect ratios*

The configurations presented above were all at aspect ratio 6.7. While larger than ARIES-CS, the aspect ratio is significantly smaller than that of the HELIAS reactor concept (Warmer *et al.* 2016) which has aspect ratio 12.2 and plasma volume of $\sim$1800 m^3.

We attempted to optimize the equilibrium at higher aspect ratios, but keeping the plasma volume equivalent to the ARIES-CS value of 450 m^3. The methodology was to begin with an internal surface of an optimized case at aspect ratio 6.7 and then scale the boundary coefficients such that the volume was equivalent. The boundary surfaces for these equilibria are shown in figure 6 and the alpha particle losses are shown in figure 7 for $0.1 < s < 0.5$. Despite the decrease in minor radius, the higher aspect ratio configurations display better confinement. At low aspect ratios, it is more difficult to meet quasihelically symmetric targets.

5. Conclusion

Results presented in this paper demonstrate that stellarator equilibria exist which have very low energetic particle losses within the half-radius with losses eliminated entirely within the $s = 0.1$ surface. Therefore, in the core, stellarator equilibria can confine energetic particles equally well to idealized axisymmetric configurations, such as tokamaks without coil ripple. This potentially eliminates one of the major concerns with stellarator reactors, namely large wall loading from prompt losses of alpha particles.

These equilibria were created using an optimization recipe that sought to minimize non-symmetric components of the magnetic field spectrum and used the Γ_c metric proposed by Nemov to minimize collisionless energetic particle losses. The results showed that optimization with both the Γ_c metric and quasihelical symmetry produced configurations with very low energetic particle losses, including the elimination of all losses within approximately the mid-radius. However, the best performing case loses some deeply trapped particles at the $s = 0.4$ surface, where other configurations do not.

https://doi.org/10.1017/S0022377819000680 Published online by Cambridge University Press

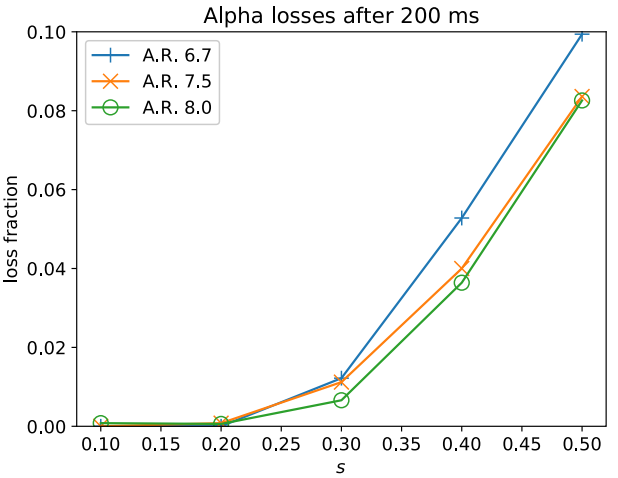

FIGURE 7. Alpha particle losses after 200 ms for three optimized configurations with different aspect ratios.

The results suggest that it is possible to achieve good energetic particle confinement despite an increase in the neoclassical metric, ϵ_{eff} by about a factor of 2 in the core. While ϵ_{eff} tends to focus on confining deeply trapped particles, energetic particles are often lost near the trapped–passing boundary. Indeed, it is possible to degrade neoclassical transport, as given by ϵ_{eff}, significantly, yet the overall energetic particle losses can be improved because of large reduction of losses near the trapped–passing boundary. This optimization can be contrasted with previous results from Ku & Garabedian (2006) and Nemov *et al.* (2014) who showed that it is possible to have improved energetic particle confinement despite reduced quasisymmetry. In Ku *et al.* this was accomplished by introducing $m = 0$, $n = 3$ and $m = 1$, $n = 3$ modes in order to improve energetic particle confinement. In Nemov *et al.* it was accomplished by increasing the number of modular coils to reduce the coil-ripple term.

This paper represents new progress on energetic particle confinement optimization in stellarators. Stellarator equilibrium optimization always requires trade-offs between different desired properties. A more comprehensive analysis is needed to determine the compatibility of good energetic ion physics with other confinement properties. It may be true that other desirable properties conflict with good energetic particle confinement. A full analysis is necessary.

The calculations were performed using collisionless drift orbits which represent optimistic estimates of particle losses. More realistic simulations would include both the slowing down of the alpha particles and pitch angle scattering. Collisional calculations require knowledge of the plasma temperature and density as a function of flux surface and will be a subject of future work.

Additionally, the effect of energetic particle modes, such as those in the Alfvén eigenmode family were not considered here. Investigating alpha particle instabilities will be important for reactors. For an overview of current research on energetic particle modes in stellarators, and the possibility of achieving reduced mode drive due to operation at higher density, see § 2.5 of Gates *et al.* (2018).

Also, all the quasihelically symmetric equilibria presented were vacuum magnetic configurations. A requirement for quasisymmetric equilibria is that good confinement is needed from the starting vacuum configuration up to the full performance with both

https://doi.org/10.1017/S0022377819000680 Published online by Cambridge University Press

finite β effects and bootstrap currents. Producing such equilibria was not attempted here.

So far, all the results presented are for idealized configurations that do not include the effects of magnetic field coils. Just as in tokamaks, coils produce additional ripple-trapped particles and constitute an additional loss mechanism. The coil-ripple effect is important, but was beyond the scope of this paper. Nevertheless, we describe here two possible methods of addressing the coil-ripple effects.

One of the more difficult aspects of stellarator coil design is maximizing the coil–plasma distance. In a reactor, the minimum size of the device will most likely be set by the neutronics blanket that must be between the vacuum and the plasma. A key parameter is the minimal coil–plasma separation distance, and this is a target to maximize (El-Guebaly *et al.* 2005). It is possible to identify regions where coil position is most sensitive (Landreman & Paul 2018; Paul *et al.* 2018), and it may be possible to target equilibria to relax specific regions such as those with strong concavities (see § 7 of Paul *et al.* 2018). Furthermore, in regions where the coil's position is less sensitive, such as the low-field side on the outside of the device, it is possible to move coils further away. This should lower the coil ripple in these regions and the expectation is that it should lower alpha particle losses from ripple-trapped particles.

A second approach is to use ferritic inserts for stellarators similar to the use in tokamaks (Shinohara *et al.* 2012). Ferritic inserts have so far not been designed for stellarators, and it is an open area of research. This could be a promising approach to reduce coil-ripple losses.

Acknowledgements

The work for this paper was supported by DE-FG02-93ER54222, DE-FG02-99ER54546 and UW 2020 135AAD3116.

REFERENCES

ANDERSON, F. S. B., ALMAGRI, A. F., ANDERSON, D. T., MATTHEWS, P. G., TALMADGE, J. N. & SHOHET, J. L. 1995 The helically symmetric experiment, (HSX) goals, design and status. *Fusion Technol.* **27** (3T), 273–277.

BOOZER, A. H. 1982 Establishment of magnetic coordinates for a given magnetic field. *Phys. Fluids* **25** (3), 520–521.

BRENT, R. P. 2013 *Algorithms for Minimization without Derivatives*. Courier Corporation.

CARY, J. R., HEDRICK, C. L. & TOLLIVER, J. S. 1988 Orbits in asymmetric toroidal magnetic fields. *Phys. Fluids* **31** (6), 1586–1600.

CONNOR, J. W. & HASTIE, R. J. 1974 Neoclassical diffusion in an $l = 3$ stellarator. *Phys. Fluids* **17** (1), 114–123.

DREVLAK, M., BEIDLER, C. D., GEIGER, J., HELANDER, P. & TURKIN, Y. 2018 Optimisation of stellarator equilibria with rose. *Nucl. Fusion* **59** (1), 016010.

DREVLAK, M., GEIGER, J., HELANDER, P. & TURKIN, Y. 2014 Fast particle confinement with optimized coil currents in the W7-X stellarator. *Nucl. Fusion* **54** (7), 073002.

EL-GUEBALY, L., RAFFRAY, R., MALANG, S., LYON, J. F., KU, L. P. & TEAM ARIES 2005 Benefits of radial build minimization and requirements imposed on aries compact stellarator design. *Fusion Sci. Technol.* **47** (3), 432–439.

GALEEV, A. A., SAGDEEV, R. Z., FURTH, H. P. & ROSENBLUTH, M. N. 1969 Plasma diffusion in a toroidal stellarator. *Phys. Rev. Lett.* **22** (11), 511.

GARREN, D. A. & BOOZER, A. H. 1991 Existence of quasihelically symmetric stellarators. *Phys. Fluids* B **3** (10), 2822–2834.

https://doi.org/10.1017/S0022377819000680 Published online by Cambridge University Press

GATES, D. A., ANDERSON, D., ANDERSON, S., ZARNSTORFF, M., SPONG, D. A., WEITZNER, H., NEILSON, G. H., RUZIC, D., ANDRUCZYK, D., HARRIS, J. H. *et al.* 2018 Stellarator research opportunities: a report of the national stellarator coordinating committee. *J. Fusion Energy* **37** (1), 51–94.

HELANDER, P., BEIDLER, C. D., BIRD, T. M., DREVLAK, M., FENG, Y., HATZKY, R., JENKO, F., KLEIBER, R., PROLL, J. H. E., TURKIN, Y. *et al.* 2012 Stellarator and tokamak plasmas: a comparison. *Plasma Phys. Control. Fusion* **54** (12), 124009.

HENNEBERG, S. A., DREVLAK, M., NÜHRENBERG, C., BEIDLER, C. D., TURKIN, Y., LOIZU, J. & HELANDER, P. 2019 Properties of a new quasi-axisymmetric configuration. *Nucl. Fusion* **59** (2), 026014.

HIRSHMAN, S. P. & WHITSON, J. C. 1983 Steepest-descent moment method for three-dimensional magnetohydrodynamic equilibria. *Phys. Fluids* **26** (12), 3553–3568.

KLINGER, T., ALONSO, A., BOZHENKOV, S., BURHENN, R., DINKLAGE, A., FUCHERT, G., GEIGER, J., GRULKE, O., LANGENBERG, A., HIRSCH, M. *et al.* 2016 Performance and properties of the first plasmas of wendelstein 7-x. *Plasma Phys. Control. Fusion* **59** (1), 014018.

KU, L. P. & GARABEDIAN, P. R. 2006 New classes of quasi-axisymmetric stellarator configurations. *Fusion Sci. Technol.* **50** (2), 207–215.

LANDREMAN, M. & PAUL, E. 2018 Computing local sensitivity and tolerances for stellarator physics properties using shape gradients. *Nucl. Fusion* **58** (7), 076023.

LANDREMAN, M. & SENGUPTA, W. 2018 Direct construction of optimized stellarator shapes. Part 1. Theory in cylindrical coordinates. *J. Plasma Phys.* **84** (6), 905840616.

LANDREMAN, M., SMITH, H. M., MOLLÉN, A. & HELANDER, P. 2014 Comparison of particle trajectories and collision operators for collisional transport in nonaxisymmetric plasmas. *Phys. Plasmas* **21** (4), 042503.

LIU, H., SHIMIZU, A., ISOBE, M., OKAMURA, S., NISHIMURA, S., SUZUKI, C., XU, Y., ZHANG, X., LIU, B., HUANG, J. *et al.* 2018 Magnetic configuration and modular coil design for the chinese first quasi-axisymmetric stellarator. *Plasma Fusion Res.* **13**, 3405067.

LOTZ, W., MERKEL, P., NUHRENBERG, J. & STRUMBERGER, E. 1992 Collisionless alpha-particle confinement in stellarators. *Plasma Phys. Control. Fusion* **34** (6), 1037.

MAU, T. K., KAISER, T. B., GROSSMAN, A. A., RAFFRAY, A. R., WANG, X. R., LYON, J. F., MAINGI, R., KU, L. P., ZARNSTORFF, M. C. & TEAM ARIES-CS 2008 Divertor configuration and heat load studies for the aries-cs fusion power plant. *Fusion Sci. Technol.* **54** (3), 771–786.

MIKHAILOV, M. I., SHAFRANOV, V. D., SUBBOTIN, A. A., ISAEV, M. Y., NÜHRENBERG, J., ZILLE, R. & COOPER, W. A. 2002 Improved α-particle confinement in stellarators with poloidally closed contours of the magnetic field strength. *Nucl. Fusion* **42** (11), L23.

MYNICK, H. E. 2006 Transport optimization in stellarators. *Phys. Plasmas* **13** (5), 058102.

MYNICK, H. E., BOOZER, A. H. & KU, L. P. 2006 Improving confinement in quasi-axisymmetric stellarators. *Phys. Plasmas* **13** (6), 064505.

NAJMABADI, F., RAFFRAY, A. R., ABDEL-KHALIK, S. I., BROMBERG, L., CROSATTI, L., EL-GUEBALY, L., GARABEDIAN, P. R., GROSSMAN, A. A., HENDERSON, D., IBRAHIM, A. *et al.* 2008 The aries-cs compact stellarator fusion power plant. *Fusion Sci. Technol.* **54** (3), 655–672.

NEMOV, V. V., KASILOV, S. V. & KERNBICHLER, W. 2014 Collisionless high energy particle losses in optimized stellarators calculated in real-space coordinates. *Phys. Plasmas* **21** (6), 062501.

NEMOV, V. V., KASILOV, S. V., KERNBICHLER, W. & HEYN, M. F. 1999 Evaluation of $1/\nu$ neoclassical transport in stellarators. *Phys. Plasmas* **6** (12), 4622–4632.

NEMOV, V. V., KASILOV, S. V., KERNBICHLER, W. & LEITOLD, G. O. 2005 The ∇b drift velocity of trapped particles in stellarators. *Phys. Plasmas* **12** (11), 112507.

NEMOV, V. V., KASILOV, S. V., KERNBICHLER, W. & LEITOLD, G. O. 2008 Poloidal motion of trapped particle orbits in real-space coordinates. *Phys. Plasmas* **15** (5), 052501.

NÜHRENBERG, J. & ZILLE, R. 1988 Quasi-helically symmetric toroidal stellarators. *Phys. Lett.* A **129**, 113–117.

https://doi.org/10.1017/S0022377819000680 Published online by Cambridge University Press

OKAMURA, S., MATSUOKA, K., NISHIMURA, S., ISOBE, M., NOMURA, I., SUZUKI, C., SHIMIZU, A., MURAKAMI, S., NAKAJIMA, N., YOKOYAMA, M. *et al.* 2001 Physics and engineering design of the low aspect ratio quasi-axisymmetric stellarator CHS-QA. *Nucl. Fusion* **41** (12), 1865.

PAUL, E. J., LANDREMAN, M., BADER, A. & DORLAND, W. 2018 An adjoint method for gradient-based optimization of stellarator coil shapes. *Nucl. Fusion* **58** (7), 076015.

SHINOHARA, K., TANI, K., OIKAWA, T., PUTVINSKI, S., SCHAFFER, M. & LOARTE, A. 2012 Effects of rippled fields due to ferritic inserts and ELM mitigation coils on energetic ion losses in a 15 MA inductive scenario in ITER. *Nucl. Fusion* **52** (9), 094008.

SPONG, D. A. 2015 3D toroidal physics: testing the boundaries of symmetry breaking. *Phys. Plasmas* **22** (5), 055602.

SPONG, D. A., HIRSHMAN, S. P., WHITSON, J. C., BATCHELOR, D. B., CARRERAS, B. A., LYNCH, V. E. & ROME, J. A. 1998 J* optimization of small aspect ratio stellarator/tokamak hybrid devices. *Phys. Plasmas* **5** (5), 1752–1758.

TOBITA, K., NAKAYAMA, T., KONOVALOV, S. V. & SATO, M. 2003 Reduction of energetic particle loss by ferritic steel inserts in ITER. *Plasma Phys. Control. Fusion* **45** (2), 133.

WARMER, F., BEIDLER, C. D., DINKLAGE, A., WOLF, R. *et al.* 2016 From W7-X to a helias fusion power plant: motivation and options for an intermediate-step burning-plasma stellarator. *Plasma Phys. Control. Fusion* **58** (7), 074006.

ZARNSTORFF, M. C., BERRY, L. A., BROOKS, A., FREDRICKSON, E., FU, G. Y., HIRSHMAN, S., HUDSON, S., KU, L. P., LAZARUS, E., MIKKELSEN, D. *et al.* 2001 Physics of the compact advanced stellarator NCSX. *Plasma Phys. Control. Fusion* **43** (12A), A237.

https://doi.org/10.1017/S0022377819000680 Published online by Cambridge University Press